

1 Atmospheric and oceanic controls on sea ice concentration  
2 in the Atlantic Water inflow region north of Svalbard during  
3 2012-2017

4 Version 0: *Draft of draft*

5 Authors<sup>a</sup>, Authors<sup>b</sup>

6 <sup>a</sup>Norwegian Polar Institute, Tromsø, Norway.

7 <sup>b</sup>Institute of Marine Research, Tromsø, Norway.

---

8 **Abstract**

9 Sea ice concentration along the continental margin of the Arctic Ocean is influenced  
10 by a multitude of factors including oceanic heat transport associated with advection of  
11 Atlantic Water, advection of ice from the Arctic Ocean, and local freezing and melting  
12 due to atmospheric forcing. Here, we characterize the evolution of sea ice concentra-  
13 tion in an area on the continental shelf break north of Svalbard in the period between  
14 2013 and 2017. During this period, a semi-regular seasonal pattern in sea ice concen-  
15 tration was interrupted by two anomalous seasons; a high ice anomaly during fall  
16 2014 and a low ice anomaly during spring 2016. Neither anomaly can be explained by  
17 abnormal upper ocean heat content as measured by an ocean mooring located on the  
18 shelf edge. Instead, we find that the predominant driver of interannual sea ice concen-  
19 tration variability during this period was variations in large-scale ice drift. While heat  
20 flux from the ocean cannot explain the interannual variability, it plays a large role in  
21 keeping the area ice free despite the freezing air temperatures during most of the year.  
22 These results are consistent with a budget analysis of sea ice concentration based on  
23 satellite records, which suggests that the area north of Svalbard is a major sink of sea  
24 ice advected in from the north.

---

25 **1. Introduction**

26 The fraction of the Arctic Ocean that is covered by sea ice is declining; annual  
27 mean sea ice extent in the northern hemisphere decreased at a rate of approximately

28     4.5% per decade between 1979 and 2015 (Comiso et al. 2017; see also Stroeve and  
29     Notz 2018; Kwok 2018). The details of this strong overall trend are complex, and in-  
30     clude great spatial inhomogeneities as well as substantial interannual variability (Ser-  
31     reze and Stroeve, 2015; Onarheim et al., 2018). Many physical processes impact sea  
32     ice concentration (*SIC*), and separate forcing mechanisms may determine local sea ice  
33     concentration in different areas, and on different temporal and spatial scales (Perovich  
34     and Richter-Menge, 2015; England et al., 2019). Local case studies are therefore an  
35     important supplement to the large-scale pan-Arctic picture of sea ice processes.

36     The area north and northeast of Svalbard has experienced a loss of sea ice both in  
37     spring and autumn during the satellite era (Onarheim et al., 2014, 2018), but it is also  
38     a regional maximum of interannual variability (present study, Grunseich and Wang,  
39     2016). In the 21st century, spring ice-free area north of Svalbard, sometimes labelled  
40     the *Whaler's Bay Polynya*, has expanded eastward (Tetzlaff et al., 2014; Ivanov et al.,  
41     2015). The location of the polynya coincides with the pathway of relatively warm  
42     Atlantic Water, which is transported through the eastern Fram Strait with the West  
43     Spitsbergen Current (WSC), wraps around the northeastern corner of Spitsbergen in  
44     three separate branches, and ultimately converges along the continental margin as the  
45     warm Arctic Slope Current Current (ASC), centered near the 800 m isobath (Koenig  
46     et al., 2017; Menze et al., 2019). In contrast to most of the Arctic Ocean, where AW  
47     is separated from the sea surface ocean by a strong halocline layer (Aagaard et al.,  
48     1981), AW is often found in close proximity to the surface in the area north of Svalbard  
49     (Meyer et al., 2018; Renner et al., 2018). As a result, the region experiences large  
50     ocean-atmosphere heat fluxes in winter (Cokelet et al., 2008), and it is a region where  
51     variability in ocean heat content has the potential to impact the sea ice cover directly  
52     (e.g., Onarheim et al., 2014; Ivanov and Repina, 2018; Ivanov et al., 2015; Polyakov  
53     et al., 2017).

54     Paragraph discussing the influence of other factors: air temperature anomalies,  
55     winds, sea ice drift.

56

57     Paragraph on interannual variability? Sources:

- Ocean: (Mulwijk et al., 2018; Kawasaki and Hasumi, 2016; Onarheim et al., 2014).
  - Atmosphere: Onarheim et al. (2014) (winds, primarily), Park et al. (2015); Isaksen et al. (2016)

62 The goal of this study is to examine drivers of interannual sea-ice variability around  
63 the continental shelf break north of Svalbard. A few key questions in particular moti-  
64 vated the study:

- 65 • Is the local sea ice cover in the AW inflow region directly determined by the  
66 upper ocean heat content on an interannual time scale?

67 • Which external conditions are responsible for generating *positive* fall anomalies  
68 in local SIC?

69 • Which external conditions are responsible for generating *negative* spring anom-  
70 lies in local SIC?

We focus on an area near the continental margin centered at 31.5°E, near the eastern end of the area along the continental margin which is typically ice-free during parts of the season. We use a 5-year record of subsurface temperature from an ocean mooring to examine interannual variations in local upper ocean heat content. Atmospheric temperature, winds, and sea ice advection and thickness are obtained from satellite and atmospheric reanalysis products.

## 77 2. Data and methods

## 78 2.1. Ocean mooring

As part of the A-TWAIN project, an ocean mooring was deployed at  $81^{\circ}24.2'N$ ,  $31^{\circ}13.2'E$  on the continental shelf break north of Kvitøya towards the Nansen Basin (Figure 1d). Bottom depth at this location is approximately 200 m. The mooring was first deployed in September 2012, and it was serviced and redeployed in the same location in September of 2013, 2015 and 2017 (Table 1).

	<i>Deployment 1</i>	<i>Deployment 2</i>	<i>Deployment 3</i>
<i>Dates</i>	16.09.12-17.09.13	21.09.13-17.09.15	19.09.15-19.09.17
<i>Duration</i>	366 d	726 d	730 d
<i>Logger depths</i>	104 m, 132 m	46 m, 111 m, 137 m	49 m, 129 m

Table 1: Overview of ocean mooring deployments and mean depth of instruments used in this study (calculated based on the median observed pressure).

84        The mooring was equipped with SeaBird SBE37 conductivity-temperature-pressure  
 85        (CTD) loggers located at various locations in the water column during the different de-  
 86        ployments (Table 1). The records from the loggers were interpolated to a common 10-  
 87        min time grid before further low-pass filtering was applied. Furthermore, the records  
 88        were linearly interpolated in depth to obtain fixed-depth time series from 63 m and 107  
 89        m (the maximum depths of the two upper sensors) in order to examine trends over the  
 90        study period.

91        *2.2. Sea ice and atmosphere data products*

92        Atmospheric variables (10-m wind and wind stress, 2-m air temperature and mean  
 93        sea level pressure) were extracted from the ECMWF ERA-5 global reanalysis product  
 94        (Copernicus Climate Change Service (C3S), 2017). A recent analysis by Wang et al.  
 95        (2019) shows that although this product is subject to certain biases over sea ice, it  
 96        generally performs better than its widely used predecessor ERA-Interim over the Arctic  
 97        Ocean.

98        Sea ice concentration (SIC) was obtained from the University of Bremen daily SIC  
 99        product from the Advanced Microwave Scanning Radiometer 2 (hf. *UoB AMSR2 SIC*)  
 100        based on the ASI algorithm (Spreen et al., 2008). The product has a uniform spatial res-  
 101        olution of 6.25 km. Sea ice drift (SID) was obtained from the NSIDC Polar Pathfinder  
 102        Daily 25 km EASE-Grid Sea Ice Motion Vectors product (Tschudi et al., 2019, hf.  
 103        *NSIDC SID*). Sea ice thickness (SIT) was obtained from the *CS2SMOS* blended prod-  
 104        uct of thickness estimates from CryoSat 2 and SMOS provided by the Alfred Wegener  
 105        Institute (Ricker et al., 2017b). *CS2SMOS* provides weekly averaged SIT on a 25 km  
 106        x 25 km grid, and is only available during parts of the year (Oct-Nov to Mar-Apr). All

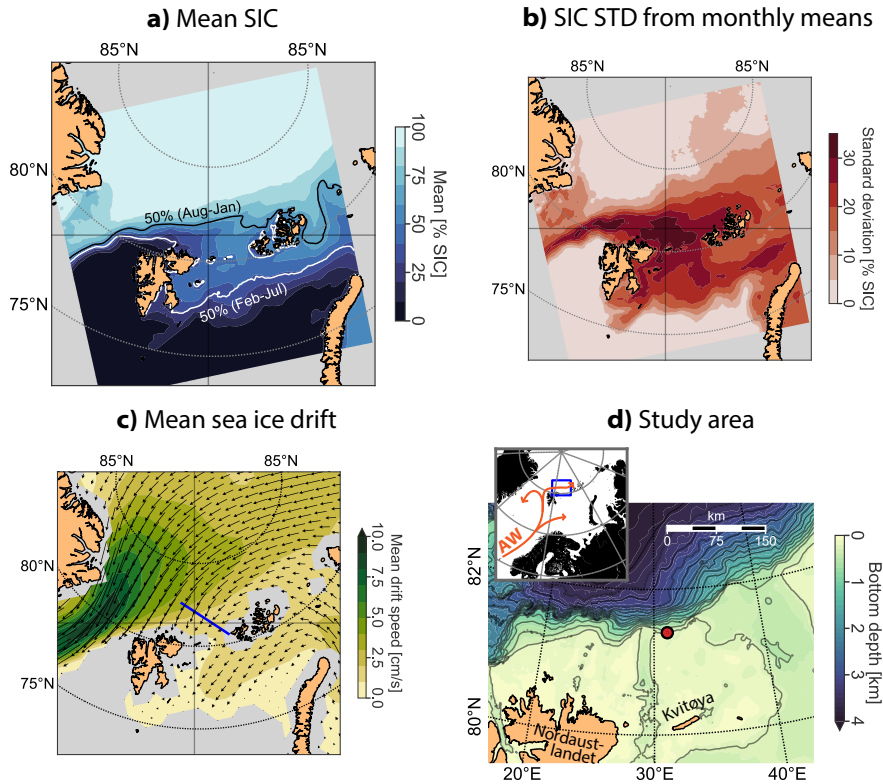


Figure 1: a) Average SIC from a subset of the UoB AMSR2 product between 02.07.2012 and 30.06.2018. The 50% SIC contour for Aug-Jan and Feb-Jul are overlaid in black and white, respectively. b) Standard deviation of monthly averaged SIC from July 2012 to June 2018, after the interannual monthly mean has been subtracted. c) Mean sea ice drift in 2012 through 2017 from the NSIDC SID product. Quiver arrows indicate the speed and direction, and are subsampled at every third grid point. Blue line shows the transect line across which sea ice fluxes are computed. d) Bathymetry from IBCAO v3 500 m x 500 m (Jakobsson et al., 2012). Contour lines are separated by 250 m. Scale bar shows lateral scale at mooring location. Inset map shows geographic location and schematic of the Atlantic Water pathways. The mooring location is indicated by the intersection of gray straight lines lines a-c and a red marker d.

107 surface variables extracted from large-scale data products were bilinearly interpolated  
108 onto the coordinates of the ocean mooring location.

109 **2.3. Seasonal sorting**

110 For the purpose of analysis, we split the year up into two halves, the *AJ* season  
111 (August through January), and the *FJ* season (February through July), where each  
112 individual season is denoted by the year of its starting month. As will be shown in  
113 Section 3.1.1 the FJ and AJ seasons approximately correspond to the high and low SIC  
114 seasons in the study area, respectively.

115 **3. Results**

116 **3.1. Ocean, ice, and atmosphere during the study period**

117 **3.1.1. Sea ice concentration and thickness**

118 The mooring location is situated in area of high seasonal and interannual SIC vari-  
119 ability (Figures 1a, b). The average fall sea ice edge (defined here as the UoB AMSR2  
120 50% SIC contour) in the AJ seasons during the study period was located north of the  
121 continental slope. In the FJ seasons, the average sea ice edge extended westward to  
122 20°E along the continental slope north of Svalbard, as well as across much of the  
123 northern Barents Sea (Figure 2). Sea ice extent also showed significant interannual  
124 variability. In particular, sea ice extent in AJ 2014 (and, to some degree, AJ 2017) was  
125 significantly greater than the AJ average, and sea ice extent in FJ 2016 was significantly  
126 less than the FJ average (Figures 2, 3a).

127 CS2SMOS sea ice thickness in the study area (Figure 3a) shows a consistent pattern  
128 of seasonal evolution throughout the record. SIT generally increased from >0.5 m in  
129 autumn/winter to between 1 and 1.5 m in spring, although the timing of the onset of  
130 the growth period was somewhat variable. A notable anomaly occurred in autumn of  
131 2017, when sea ice was unusually thick (>0.5 m) at the onset of the growth season.

132 **3.1.2. Ocean temperature**

133 Subsurface ocean temperature exhibited a strong seasonality, typically with a peaked  
134 maximum around September-October and a broader minimum in March-July (Figure

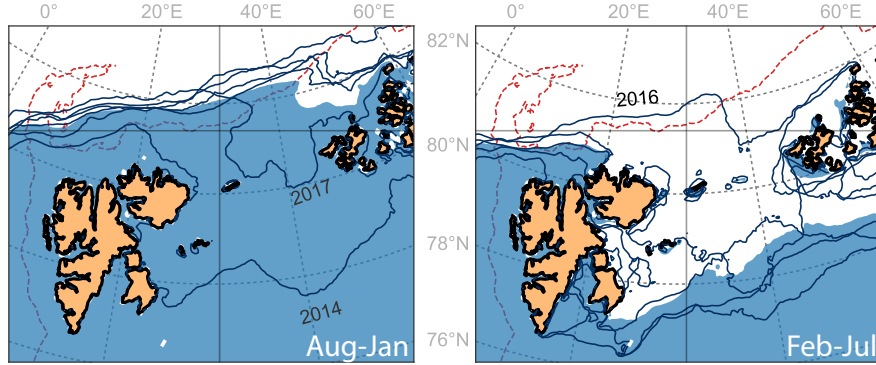


Figure 2: Extent of 50% average SIC in UoB AMSR2 during *a*: August-January and *b*: February-July. White color on blue background shows the seasonal averages over the entire period of 1/8/2012 to 31/1/2017. Black contour shows the extent for each individual season. Anomalous years are indicated with a label near the associated contour (label defined by the year of the first month of the season). Red dashed lines shows the 800 m bathymetric contour, a proxy for the pathway of AW transport. Intersection of gray lines show the mooring location.

3b). Average temperature during the AJ seasons (interpolated between sensors to a constant depth) was 2.51°C at 63 m (2014-2016) and 2.73°C at 107 m (2012-2016). The average temperature during the FJ seasons was 0.51°C at 63 m (2014-2017) and 1.18°C at 107 m (2013-2017).

Temperature generally increased with depth; during the seasons where a shallow sensor was available, interpolated ocean temperature was higher at 107 m than at 63 m (by 0.52°C in AJ and 0.73°C in FJ). In general, the temperature difference nearly vanished near the annual temperature maximum, and was greatest during the annual minimum, consistent with the influence of winter surface cooling decreasing with depth.

The temperature-salinity distribution from the AJ season (Figures 4b, d) shows that the seasonal increase in subsurface temperature was associated with an inflow of Atlantic Water. Near 130 m depth, the distribution fell almost entirely within the AW boundaries, while near 50 m, the distribution was dispersed along the  $27.8 \text{ m}^{-3}$  isopycnal, extending well into the range of Arctic Atlantic Water (typically interpreted as AW which has recirculated in the Arctic Ocean for some time), and also spreading out towards the  $27.6 \text{ m}^{-3}$  isopycnal.

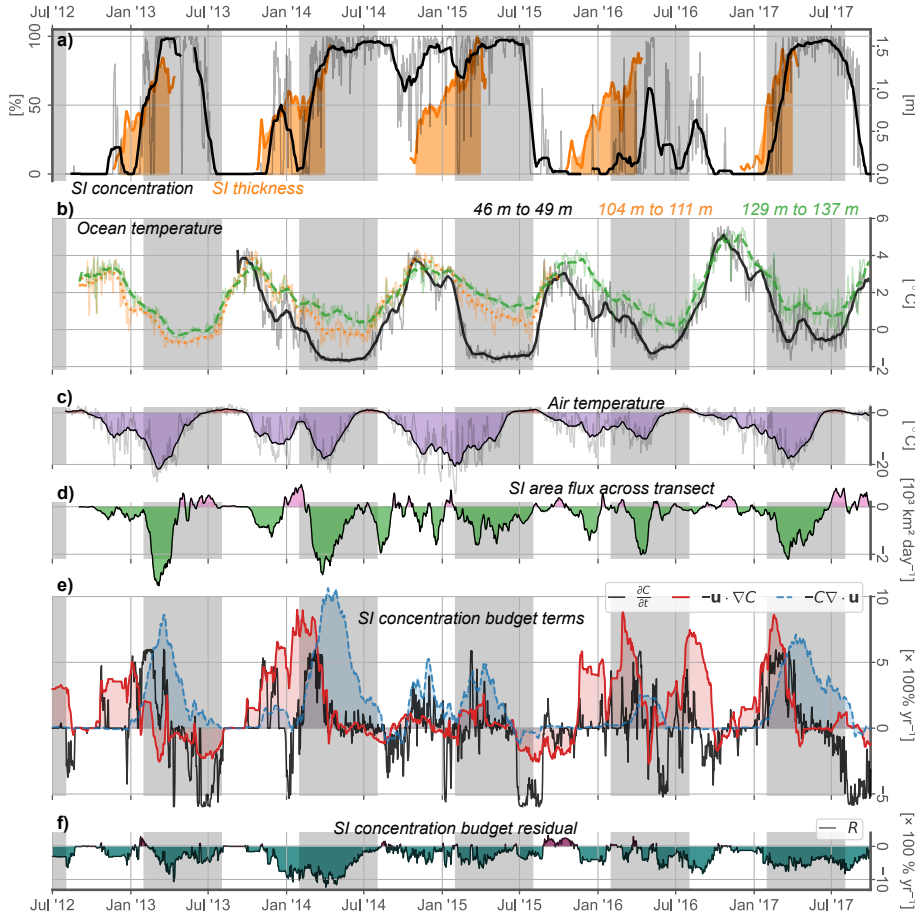


Figure 3: Time series of various variables at the mooring location. *a*: Sea ice concentration (black) and sea ice thickness (orange). *b*) Ocean temperature at various depths. *c*) Air temperature. *d*) Net sea ice drift across the large scale transect shown in Figure 1c, positive approximately northeastward (away from the mooring site). *e*) Three first terms of Equation (1) from September 2012 through September 2017. All terms are defined such that positive values indicate SIC increase. *f*) like *e*, for the residual term of Equation (1). *a-d* show 31-day running averages (thick lines) and daily means (thin faint lines). *e-f* show 61-day running averages.

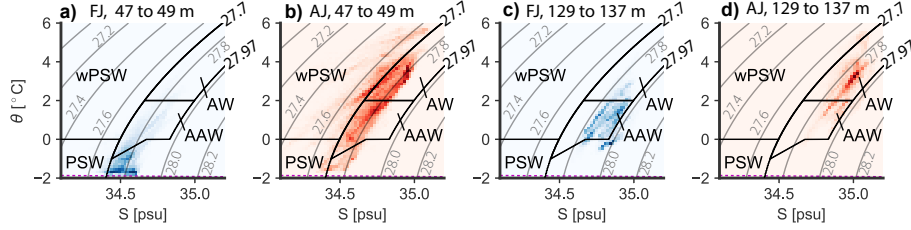


Figure 4: Normalized 2-D histograms showing the relative distribution of salinity  $S$  and potential temperature  $\theta$  from the loggers at 47 to 49 m depth (a, b), and 129 to 137 m depth (c, d), sorted by season.  $\sigma$  isopycnals shown in gray, with labels of unit  $\text{kg m}^{-3}$  and separated by  $0.2 \text{ kg m}^{-3}$ . Freezing point shown in dashed pink line. Based on all available data at 10 minute resolution. Water masses based on Rudels et al. (2005) are indicated with black lines. Note that the logger depths were similar, but slightly different, during the different deployments (Table 1).

151     In the FJ season (Figures 4a, c), the distribution from the  $\sim 130$  m logger was  
 152     largely found within in the AAW range, although temperature was occasionally colder  
 153     than the lower bound of  $0^{\circ}\text{C}$  given by Rudels et al. (2005). Nea 50 m depth, the  
 154     winter distribution was concentrated near the freezing line, particularly due to the cold  
 155     spring temperatures during 2014-2015. This suggests that a mixed layer in contact with  
 156     surface cooling and/or freezing extended down beyond 50 m during these seasons.

157     Ocean temperature below the ice cover increased between 2014 and 2017; dur-  
 158     ing this period, average July temperatures interpolated to 63 m depth increased at a  
 159     rate of  $0.29^{\circ}\text{C year}^{-1}$  ( $R^2 = 0.98$ ). At 107 m depth, the corresponding trend over the  
 160     same years increased as well, but less uniformly so ( $0.21^{\circ}\text{C year}^{-1}$ ,  $R^2 = 0.63$ ). Ad-  
 161     ditional observations would be necessary to determine whether this trend is related to  
 162     e.g. increased vertical mixing, or an increase in the summer temperature of the WSC.  
 163     No clear trend was observed in autumn temperatures, although interannual differences  
 164     were clearly present, as shown e.g. in the anomalously warm peak in October 2016,  
 165     where monthly mean subsurface temperature exceeded  $4.9^{\circ}\text{C}$  at both 63 m and 107 m.

### 166     3.1.3. Air temperature and winds

167     Both near-surface air temperature and wind speed at the mooring location exhibited  
 168     clear seasonality during the study period (Figure 3c; Supporting information, Figure

169 8). During all years, monthly averaged air temperature ( $^{\circ}\text{C}$ ) was positive in summer  
170 (somewhere between June and August), and in most years air temperatures reached  
171 a clear minimum in winter. The year 2016 was abnormally warm; the average air  
172 temperature in 2016 ( $-3.4^{\circ}\text{C}$ ) was  $3.5^{\circ}\text{C}$  warmer than the annual average during the  
173 four other seasons ( $-6.9^{\circ}\text{C}$ ), largely due to anomalously warm spring temperatures.  
174 The minimum monthly averaged air temperature was  $-10.2^{\circ}\text{C}$  during 2016, compared  
175 to  $-17.7^{\circ}\text{C}$  to  $-21.8^{\circ}\text{C}$  during the four other full years.

176 The seasonal pattern in wind speed was similar during all years; in general, monthly  
177 averaged wind speed decreased during the first half of the year and increased during  
178 the second, within a range of  $\sim 5$  m/s to  $\sim 10$  m/s.

179 *3.1.4. Sea ice drift*

180 The study site is located near the margin of the Transpolar Drift Stream, and sea  
181 ice is generally advected towards the site from the north and east (Figure 1c). Con-  
182 sequently, the record of sea ice area advection across the reference transect was pre-  
183 dominantly oriented in the negative direction (towards the study site) during the study  
184 period (Figure 3d). Average area flux across the 375 km long transect between 2012  
185 and 2017 was  $-1.34 \times 10^5 \text{ km}^2 \text{ year}^{-1}$ . For context, this amounts to an annual area flux  
186 of slightly more than twice the land area of the Svalbard archipelago ( $6.1 \times 10^4 \text{ km}^2$ ).

187 Sea ice advection across the transect was seasonally biased towards the FJ season.  
188 It was concentrated in intraseasonal pulses near the onset of the sea ice cover period  
189 in late winter/early spring, but there was considerable interannual variability, with a  
190 maximum FJ net flux in 2014 ( $>800 \text{ km}^2 \text{ day}^{-1}$ ), and a minimum ( $<500 \text{ km}^2 \text{ day}^{-1}$ ) in  
191 2016. The net flux during the AJ season also had a clear maximum in 2014 ( $\sim 500 \text{ km}^2$   
192  $\text{day}^{-1}$ ) and a clear minimum in 2016 ( $<50 \text{ km}^2 \text{ day}^{-1}$ ).

193 *3.2. High SIC anomaly during autumn 2014*

194 In contrast to the rest of the 2012-2017 period, the study area remained largely ice  
195 covered through the AJ season of 2014 (Figure 3a). The mean sea ice edge (opera-  
196 tionally defined here as the 50% SIC contour) along the AW inflow pathway north of  
197 Svalbard was in AJ 2014 situated north of Nordaustlandet at  $<20^{\circ}\text{E}$ , more than 400 km

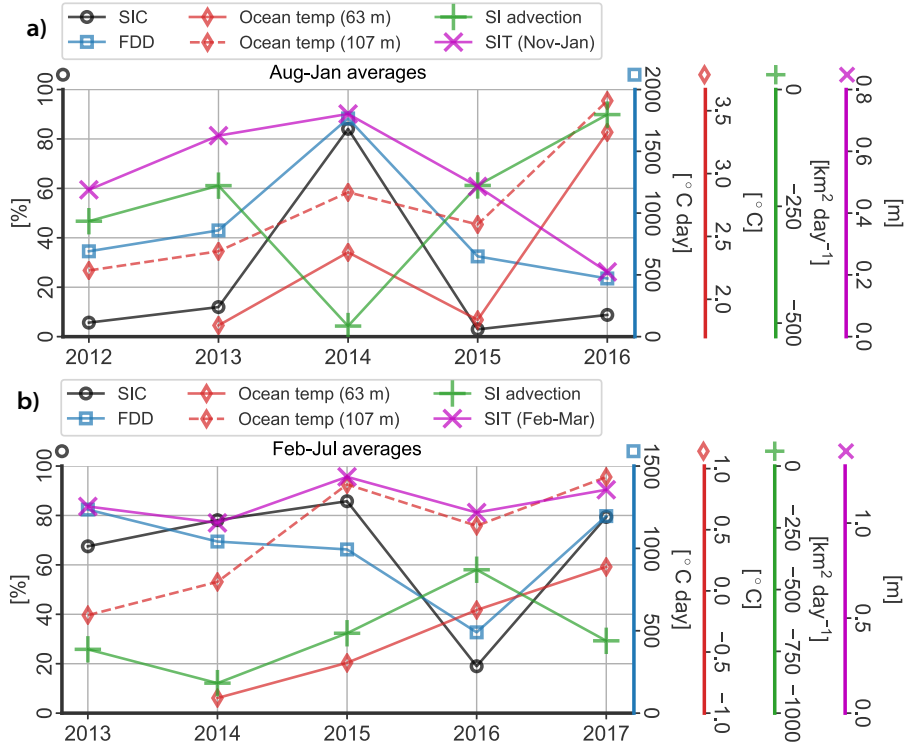


Figure 5: Seasonal average quantities from a: August through January and b: February through July.

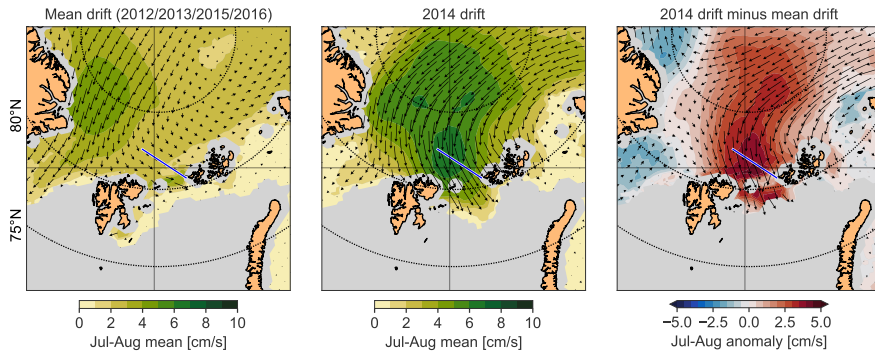


Figure 6: Mean sea ice drift in July through August: a: Mean for the 2012, 2013, 2015, and 2016 seasons. b: Mean for the 2014 season. c: b minus a. Flux transect shown in blue. Intersection of gray lines show the mooring location.

198 west of its typical AJ location north of Franz Josef Land at >44°E (Figure 2a). The sea  
199 ice cover also extended across the northern Barents Sea, which was otherwise largely  
200 ice free autumn during the study period.

201 We find no indication that the local upper ocean heat content was particularly low  
202 during the 2014 AJ season, or during the preceding 2014 FJ season. We do, however,  
203 note that air temperatures were anomalously low and, as a result, the number of freez-  
204 ing degree days during the 2014 AJ season was approximately double that of the  
205 other AJ seasons. However, the low air temperatures may in part *result* from the high  
206 sea ice cover, as sea ice can have a large cooling effect on the atmosphere even at rel-  
207 atively small spatial scales around Svalbard (Isaksen et al., 2016). Since anomalously  
208 high SIC in late summer preceded the anomalous temperature drop (in early autumn),  
209 we cannot attribute the anomalously high autumn SIC to local sea ice growth, although  
210 it is likely that the low air temperatures contributed to additional sea ice formation  
211 during the period.

212 To explain the high SIC in late summer, we note that AJ sea ice advection from the  
213 north was more than twice as great in 2014 compared to 2013 (Figure 5a). Much of this  
214 sea ice advection occurred through July and early August, during what is typically the  
215 melt season (Figure 3d). During this time, there was a strong southward drift through-  
216 out the Atlantic Section of the Arctic Ocean (Figure 6), with the entire Transpolar Drift  
217 Stream intensifying and curving to the left away from its usual outlet in the Fram Strait  
218 and towards the Barents Sea.

219 Based on the time series, a plausible interpretation is therefore that the continued  
220 supply of sea ice advected from the north counteracted the seasonal melting, and pre-  
221 vented the disappearance of the sea ice north of Svalbard during late summer 2014.  
222 The resulting reduced heat flux from the ocean to the atmosphere resulted in an unusu-  
223 ally rapid cooling of the air, which in turn may have contributed to increased sea ice  
224 growth during the AJ season of 2014.

### 225 3.3. Low SIC anomaly during spring 2016

226 Sea ice concentration in the study region was very low (~20%) during the FJ season  
227 of 2016 compared to the four other seasons (~80%, Figure 5b). The mean ice edge

228 was located near its typical location during the AJ season, north and east of the study  
 229 area (Figure 2). Upper ocean temperature was higher in February 2016 compared to  
 230 previous years, suggesting that increased upward heat flux may have contributed to  
 231 limiting ice formation. However, since sea ice did increase during the FJ 2017 season  
 232 despite similarly high February upper ocean temperatures, it is unlikely that increased  
 233 upper heat content was the main driver of the 2016 sea ice minimum in the study area.

234 The sea ice anomaly coincided with interannual FJ 2016 minima both in sea ice  
 235 advection from the northeast (60% of the FJ 2017 value) and number of freezing de-  
 236 gree days (41% of the FJ 2017 value). As discussed in Section 3.2, air temperature and  
 237 sea ice concentration are strongly related through a feedback cycle, and the relatively  
 238 low flux of sea ice into the area will likely have contributed to higher local air temper-  
 239 atures and less local sea ice formation. However, the 2016 spring season was a year of  
 240 anomalously high air temperatures and low sea ice extent across the Arctic Ocean, as  
 241 has been discussed in several other studies (e.g. Ricker et al., 2017a; Petty et al., 2018;  
 242 Stroeve et al., 2018).

### 243 3.4. Sea ice concentration budget

244 Having considered the characteristics of the various time series, we then examined  
 245 the evolution of SIC in the area more quantitatively by constructing a sea ice concentra-  
 246 tion budget for the broader area. We followed the methodology developed by Holland  
 247 and Kimura (2016), decomposing the time evolution of the local sea ice concentration  
 248 for each spatial point, denoted by the subscript  $i$ :

$$\underbrace{\frac{\partial C_i}{\partial t}}_{\text{Intensification}} = \underbrace{-\mathbf{u}_i \cdot \nabla C_i}_{\text{Advection}} - \underbrace{C_i \nabla \cdot \mathbf{u}_i}_{\text{Convergence}} + \underbrace{R_i}_{\text{Residual}} \quad (1)$$

249 where  $C$  denotes the sea ice concentration,  $\mathbf{u}$  is the local drift vector, and  $R_i$  is  
 250 a residual which includes local sea ice concentration changes due to local freezing,  
 251 melting and deformation (e.g. ridging).

252 We evaluated Equation 1 daily at each point of the native 25 km x 25 km grid of  
 253 the NSIDC SID product, from which we obtained  $\mathbf{u}$ .  $C$  was obtained from UoB SIC  
 254 bilinearly interpolated onto the NSIDC SID grid.

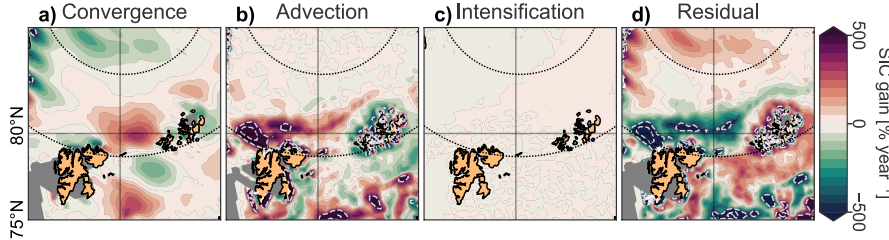


Figure 7: *a-d*) Average terms of Equation (1) from September 2012 through September 2017: *a*) Convergence,  $-C\nabla \cdot \mathbf{u}$ , *b*) advection,  $-\mathbf{u} \cdot \nabla C$ , *c*) intensification,  $\frac{\partial C}{\partial t}$ , and *d*) residual,  $R$ . All terms are defined such that positive values (red) indicate SIC *gain*, and negative values (green) indicate SIC *loss*. Color scale saturated at  $\pm 500 \text{ \% year}^{-1}$ ; beyond this, white dashes contours are shown at intervals of  $500 \text{ \% year}^{-1}$ . The mooring location is indicated by the intersection of the straight gray lines.

255 The SIC budget at the mooring location was dominated by flux divergence, with  
 256 the advection and divergence terms dominateing during various times during the study  
 257 period (Figure 3e). The residual term (Figure 3f) was negative throughout most of the  
 258 record. Assuming that the influence of ridging and other forms of deformation was  
 259 minor, this suggests that the study area was a sink of sea ice collected in the region by  
 260 large-scale sea ice drift.

261 Clear spatial patterns emerge when the SIC budget is considered over the greater  
 262 region surrounding the mooring site (Figure 7). The area north and northeast of Sval-  
 263 bard experienced a large net positive contribution to SIC from advection of SIC and  
 264 convergence of the sea ice drift. The advection term was greatest in the west, with  
 265 a maximum approximately over the Yermak Pass. The convergence term was great-  
 266 est north of the passage into the Barents Sea between Nordaustlandet and Franz Josef  
 267 Land.

268 Since the intensification term is negligible when summed over long time scales, the  
 269 residual term must balance total flux divergence. As a result, the residual term, which  
 270 includes concentration changes due to freezing/melting, is negative along the an area  
 271 extending from the Yermak Pass in the west and past Franz Josef Land in the east, along  
 272 a trajectory correspondig approximately to the continental margin and the pathway of  
 273 AW.

274     **4. Summary and discussion**

275       Unfinished, and currently only in bullet point form.

276     *4.1. Characterization*

- 277       • Quick summary of the data.  
278       • In particular, mooring data (water masses, temperature ranges, variability).  
279       • SIC anomalies.

280     *4.2. Anomalies*

- 281       • Both spring 2014 and autumn 2016 were anomalous across the entire Arctic.  
282       • AJ2014: The local anomaly was related to an anomalously strong and eastward  
283           deflected TPD. (The sudden inflow of sea ice kept the air cold, preventing addi-  
284           tional melt?)  
285       • FJ2016: Cold air temperatures (across the arctic). Advection was at its smallest  
286           across the FJ seasons.  
287       • Have been connected to large-scale atmospheric anomalies - discuss *briefly*.

288     *4.3. Role of AW*

- 289       • No obvious connection between upper ocean heat and local SIC on sub-annual  
290           time scales.  
291       • Acknowledge:  
292           – These single point instruments are probably not a great proxy for upper  
293           ocean heat in the broader area.  
294           – Heat fluxes to the surface are extremely dependent on the near-surface strat-  
295           ification, which we have no information about.

- 296     ● The spatial structure of the residual term (which can be seen as a rough proxy  
297       for melting/freezing) roughly matches the distribution of AW (...!). (*However*, it  
298       may be more coincidental in the sense that these maxima will occur wherever  
299       the SI edge is.. ). (But, Holland and Kimura (2016) do seem to have a maximum  
300       above Svalbard - also in comparison with other places along the edge..).

301     **4.4. Sea ice concentration in the area north of Svalbard**

- 302     ● Sea ice drift is a key driver of interannual variability.  
303     ● Clear correlation between SIC and temperature locally. It looks like drift from  
304       the north tends to precede temperature drops (maybe drift is the driver, but the  
305       feedback loop with the atmosphere amplifies the effect?).  
306     ● Persistent patterns of advective and convergence terms due to land constraints?  
307       And AW melting?

308     **4.5. Open questions**

- 309     ● How *thick* is the ice? Missing SIT in the budget..  
310     ● What governs the episodic deflection of drift towards this area?  
311     ● Missing the very surface layer, so we can't really constrain the heat flux..  
312     ● Along the same lines: Haven't looked at wind-driven mixing or upwelling..  
313     ● Is there a potential for predictability on interannual time scales?

314     **5. Various notes that may eventually find a home in the discussion section**

315     *Notes on the 2014 season:* In the Arctic Ocean as a whole, the winter seasons of  
316     2013 and 2014 were anomalously cold (Tilling et al., 2015). While total Arctic autumn  
317     sea ice volume during these two seasons was elevated compared to the preceding and  
318     following ones, the spatial pattern of sea ice extent differed markedly between 2013  
319     and 2014, with the mean ice edge extending much farther south in the Barents and  
320     Kara Sea sections of the Arctic Ocean during autumn 2014 (Serreze et al., 2016).

321 During the 2014 fall season, the study region remained largely sea ice covered, despite  
322 high subsurface ocean temperature. During the period where sea ice concentration  
323 typically decreases (June-August), neither subsurface ocean temperature nor air tem-  
324 perature were particularly low compared to other years. Instead, the clearest anomaly  
325 was an unusually strong sea ice advection in late summer, with a sustained sea ice drift  
326 from the northeast starting July 25 through August 2, reaching a maximum of  $X \text{ km}^2$   
327  $\text{m}^{-1} \text{ day}^{-1}$  on August 17th. Sea ice drift into the area remained relatively high during  
328 the fall season, with the AJ season of 2014.

329

- 330 • Tiller et al: Low sea ice volume result of warm summer. (In turn a result of  
331 increased IR due to import of moisture/whatever?)
- 332 • There was plenty of heat in the ocean.
- 333 • AJ sea ice advection was high through the AJ season. In particular, there was a  
334 large advection event during the melt season, which may have offset the meelt-  
335 ing?.
- 336 • The elevated summer advection was associated with an intensification, and left-  
337 ward deflection, of the transpolar drift (large scale!).
- 338 • Air temperature was low.

339 *Notes on 2016 context:*

- 340 • Petty et al: Very low AO cover in the FJ season (but pretty high in AJ)!. The  
341 high in AJ is attributed to compacting by cyclones.
- 342 • Boisvert et al: Extreme cyclone in Jan 2016 responsible for reduced sea ice in  
343 Barents and Kara Seas.
- 344 • Ricker et al: Attribute the low SIC to
  - 345 1. Loss of sea ice in summer 2015
  - 346 2. Lack of SI growth in winter due to unusually warm winter 2016

- 347     ● Air temperature was high/FDD was about half what it usually is.
- 348     ● The ocean was \*a little\* warmer? (Although the following year, the ocean was  
349       also kind of warm.).
- 350     ● FJ sea ice advection was lower than usual (although not compared to 2014, when  
351       sea ice cover was already high in winter).
- 352     ● Stroeve and Notz (2018) showed that the onset of melt in the northern Barents  
353       Sea occurred earlier than ever before in the satellite record, nearly a month earlier  
354       than the 1981-2010 mean.

355     **References**

- 356     Aagaard, K., Coachman, L.K., Carmack, E., 1981. On the halocline of the Arctic  
357       Ocean. Deep Sea Research Part A. Oceanographic Research Papers 28, 529–545.  
358       doi:10.1016/0198-0149(81)90115-1.
- 359     Cokelet, E.D., Tervalon, N., Bellingham, J.G., 2008. Hydrography of the West Spits-  
360       bergen Current, Svalbard Branch: Autumn 2001. Journal of Geophysical Research:  
361       Oceans 113. doi:10.1029/2007JC004150.
- 362     Comiso, J.C., Meier, W.N., Gersten, R., 2017. Variability and trends in the Arctic  
363       Sea ice cover: Results from different techniques. Journal of Geophysical Research:  
364       Oceans 122, 6883–6900. doi:10.1002/2017JC012768.
- 365     Copernicus Climate Change Service (C3S), 2017. ERA5: Fifth genera-  
366       tion of ECMWF atmospheric reanalyses of the global climate. Coperni-  
367       cus Climate Change Service Climate Data Store (CDS), accessed 2019-11-11.  
368       <https://cds.climate.copernicus.eu/cdsapp#!/home>.
- 369     England, M., Jahn, A., Polvani, L., 2019. Nonuniform Contribution of Internal  
370       Variability to Recent Arctic Sea Ice Loss. Journal of Climate 32, 4039–4053.  
371       doi:10.1175/JCLI-D-18-0864.1.

- 372 Grunseich, G., Wang, B., 2016. Predictability of Arctic Annual Minimum Sea Ice  
373 Patterns. *Journal of Climate* 29, 7065–7088. doi:10.1175/JCLI-D-16-0102.1.
- 374 Holland, P.R., Kimura, N., 2016. Observed Concentration Budgets of Arctic and  
375 Antarctic Sea Ice. *Journal of Climate* 29, 5241–5249. doi:10.1175/JCLI-D-16-  
376 0121.1.
- 377 Isaksen, K., Nordli, Ø., Førland, E.J., Łupikasza, E., Eastwood, S., Niedzwiedź, T.,  
378 2016. Recent warming on Spitsbergen—Influence of atmospheric circulation and  
379 sea ice cover. *Journal of Geophysical Research: Atmospheres* 121, 11,913–11,931.  
380 doi:10.1002/2016JD025606.
- 381 Ivanov, V., Alexeev, V., Koldunov, N.V., Repina, I., Sandø, A.B., Smedsrød, L.H.,  
382 Smirnov, A., 2015. Arctic Ocean Heat Impact on Regional Ice Decay: A Sug-  
383 gested Positive Feedback. *Journal of Physical Oceanography* 46, 1437–1456.  
384 doi:10.1175/JPO-D-15-0144.1.
- 385 Ivanov, V.V., Repina, I.A., 2018. The Effect of Seasonal Variability of Atlantic Water  
386 on the Arctic Sea Ice Cover. *Izvestiya, Atmospheric and Oceanic Physics* 54, 65–72.  
387 doi:10.1134/S0001433818010061.
- 388 Jakobsson, M., Mayer, L., Coakley, B., Dowdeswell, J.A., Forbes, S., Fridman,  
389 B., Hodnesdal, H., Noormets, R., Pedersen, R., Rebesco, M., Schenke, H.W.,  
390 Zarayskaya, Y., Accettella, D., Armstrong, A., Anderson, R.M., Bienhoff, P., Camer-  
391 lenghi, A., Church, I., Edwards, M., Gardner, J.V., Hall, J.K., Hell, B., Hestvik, O.,  
392 Kristoffersen, Y., Marcussen, C., Mohammad, R., Mosher, D., Nghiem, S.V., Pe-  
393 drosa, M.T., Travaglini, P.G., Weatherall, P., 2012. The International Bathymetric  
394 Chart of the Arctic Ocean (IBCAO) Version 3.0. *Geophysical Research Letters* 39.  
395 doi:10.1029/2012GL052219.
- 396 Kawasaki, T., Hasumi, H., 2016. The inflow of Atlantic water at the Fram Strait and  
397 its interannual variability. *Journal of Geophysical Research: Oceans* 121, 502–519.  
398 doi:10.1002/2015JC011375.

- 399 Koenig, Z., Provost, C., Sennéchal, N., Garric, G., Gascard, J.C., 2017. The Yermak  
400 Pass Branch: A Major Pathway for the Atlantic Water North of Svalbard? *Journal*  
401 *of Geophysical Research: Oceans* 122, 9332–9349. doi:10.1002/2017JC013271.
- 402 Kwok, R., 2018. Arctic sea ice thickness, volume, and multiyear ice coverage: Losses  
403 and coupled variability (1958–2018). *Environmental Research Letters* 13, 105005.  
404 doi:10.1088/1748-9326/aae3ec.
- 405 Menze, S., Ingvaldsen, R.B., Haugan, P., Fer, I., Sundfjord, A., Beszczynska-Moeller,  
406 A., Falk-Petersen, S., 2019. Atlantic Water Pathways Along the North-Western Sval-  
407 bard Shelf Mapped Using Vessel-Mounted Current Profilers. *Journal of Geophysical*  
408 *Research: Oceans* 124, 1699–1716. doi:10.1029/2018JC014299.
- 409 Meyer, A., Fer, I., Sundfjord, A., Peterson, A.K., 2018. Mixing rates and vertical  
410 heat fluxes north of Svalbard from Arctic winter to spring. *Journal of Geophysical*  
411 *Research: Oceans* , 4569–4586doi:10.1002/2016JC012441@10.1002/(ISSN)2169-  
412 9291.NICE1.
- 413 Muilwijk, M., Smedsrød, L.H., Ilicak, M., Drange, H., 2018. Atlantic Water Heat  
414 Transport Variability in the 20th Century Arctic Ocean From a Global Ocean Model  
415 and Observations. *Journal of Geophysical Research: Oceans* 123, 8159–8179.  
416 doi:10.1029/2018JC014327.
- 417 Onarheim, I.H., Eldevik, T., Smedsrød, L.H., Stroeve, J.C., 2018. Seasonal and Re-  
418 gional Manifestation of Arctic Sea Ice Loss. *Journal of Climate* 31, 4917–4932.  
419 doi:10.1175/JCLI-D-17-0427.1.
- 420 Onarheim, I.H., Smedsrød, L.H., Ingvaldsen, R.B., Nilsen, F., 2014. Loss of sea ice  
421 during winter north of Svalbard. *Tellus A: Dynamic Meteorology and Oceanography*  
422 66, 23933. doi:10.3402/tellusa.v66.23933.
- 423 Park, D.S.R., Lee, S., Feldstein, S.B., 2015. Attribution of the Recent Winter Sea  
424 Ice Decline over the Atlantic Sector of the Arctic Ocean. *Journal of Climate* 28,  
425 4027–4033. doi:10.1175/JCLI-D-15-0042.1.

- 426 Perovich, D.K., Richter-Menge, J.A., 2015. Regional variability in sea ice melt in a  
427 changing Arctic. Philosophical Transactions of the Royal Society A: Mathematical,  
428 Physical and Engineering Sciences 373, 20140165. doi:10.1098/rsta.2014.0165.
- 429 Petty, A.A., Stroeve, J.C., Holland, P.R., Boisvert, L.N., Bliss, A.C., Kimura, N., Meier,  
430 W.N., 2018. The Arctic sea ice cover of 2016: A year of record-low highs and  
431 higher-than-expected lows. The Cryosphere 12, 433–452.
- 432 Polyakov, I.V., Pnyushkov, A.V., Alkire, M.B., Ashik, I.M., Baumann, T.M., Carmack,  
433 E.C., Gosczko, I., Guthrie, J., Ivanov, V.V., Kanzow, T., Krishfield, R., Kwok, R.,  
434 Sundfjord, A., Morison, J., Rember, R., Yulin, A., 2017. Greater role for Atlantic  
435 inflows on sea-ice loss in the Eurasian Basin of the Arctic Ocean. Science 356,  
436 285–291. doi:10.1126/science.aai8204.
- 437 Renner, A.H.H., Sundfjord, A., Janout, M.A., Ingvaldsen, R.B., Beszczynska-Möller,  
438 A., Pickart, R.S., Pérez-Hernández, M.D., 2018. Variability and Redistribution of  
439 Heat in the Atlantic Water Boundary Current North of Svalbard. Journal of Geo-  
440 physical Research: Oceans 123, 6373–6391. doi:10.1029/2018JC013814.
- 441 Ricker, R., Hendricks, S., Girard-Ardhuin, F., Kaleschke, L., Lique, C., Tian-Kunze,  
442 X., Nicolaus, M., Krumpen, T., 2017a. Satellite-observed drop of Arctic sea  
443 ice growth in winter 2015–2016. Geophysical Research Letters 44, 3236–3245.  
444 doi:10.1002/2016GL072244.
- 445 Ricker, R., Hendricks, S., Kaleschke, L., Tian-Kunze, X., King, J., Haas, C., 2017b.  
446 A weekly Arctic sea-ice thickness data record from merged CryoSat-2 and SMOS  
447 satellite data. The Cryosphere 11, 1607–1623. doi:<https://doi.org/10.5194/tc-11-1607-2017>.
- 449 Rudels, B., Björk, G., Nilsson, J., Winsor, P., Lake, I., Nohr, C., 2005. The interaction  
450 between waters from the Arctic Ocean and the Nordic Seas north of Fram Strait and  
451 along the East Greenland Current: Results from the Arctic Ocean-02 Oden expedi-  
452 tion. Journal of Marine Systems 55, 1–30. doi:10.1016/j.jmarsys.2004.06.008.

- 453 Serreze, M.C., Stroeve, J., 2015. Arctic sea ice trends, variability and impli-  
454 cations for seasonal ice forecasting. Philosophical Transactions of the Royal  
455 Society A: Mathematical, Physical and Engineering Sciences 373, 20140159.  
456 doi:10.1098/rsta.2014.0159.
- 457 Serreze, M.C., Stroeve, J., Barrett, A.P., Boisvert, L.N., 2016. Summer atmospheric  
458 circulation anomalies over the Arctic Ocean and their influences on September sea  
459 ice extent: A cautionary tale. Journal of Geophysical Research: Atmospheres 121,  
460 11,463–11,485. doi:10.1002/2016JD025161.
- 461 Spreen, G., Kaleschke, L., Heygster, G., 2008. Sea ice remote sensing using  
462 AMSR-E 89-GHz channels. Journal of Geophysical Research: Oceans 113.  
463 doi:10.1029/2005JC003384.
- 464 Stroeve, J., Notz, D., 2018. Changing state of Arctic sea ice across all seasons. Envi-  
465 ronmental Research Letters 13, 103001. doi:10.1088/1748-9326/aade56.
- 466 Stroeve, J.C., Schroder, D., Tsamados, M., Feltham, D., 2018. Warm winter, thin ice?  
467 The Cryosphere 12, 1791–1809.
- 468 Tetzlaff, A., Lüpkes, C., Birnbaum, G., Hartmann, J., Nygard, T., Vihma, T., 2014.  
469 Brief Communication: Trends in sea ice extent north of Svalbard and its impact  
470 on cold air outbreaks as observed in spring 2013. The Cryosphere 8, 1757–1762.  
471 doi:<https://doi.org/10.5194/tc-8-1757-2014>.
- 472 Tilling, R.L., Ridout, A., Shepherd, A., Wingham, D.J., 2015. Increased Arctic sea  
473 ice volume after anomalously low melting in 2013. Nature Geoscience 8, 643–646.  
474 doi:10.1038/ngeo2489.
- 475 Tschudi, M., Meier, W.N., Stewart, J.S., Fowler, C., Maslanik, J., 2019. Polar  
476 Pathfinder Daily 25 km EASE-Grid Sea Ice Motion Vectors, Version 4 (hourly, single  
477 levels). Boulder, Colorado, USA. NASA National Snow and Ice Data Center Dis-  
478 tributed Active Archive Center. doi:10.1029/2018JC014299. Accessed 11.11 2019.
- 479 Wang, C., Graham, R.M., Wang, K., Gerland, S., Granskog, M.A., 2019. Compara-  
480 tion of ERA5 and ERA-Interim near-surface air temperature, snowfall and precipi-

<sup>481</sup> tation over Arctic sea ice: Effects on sea ice thermodynamics and evolution. The  
<sup>482</sup> Cryosphere 13, 1661–1679. doi:<https://doi.org/10.5194/tc-13-1661-2019>.

**483 6. Additional figures**

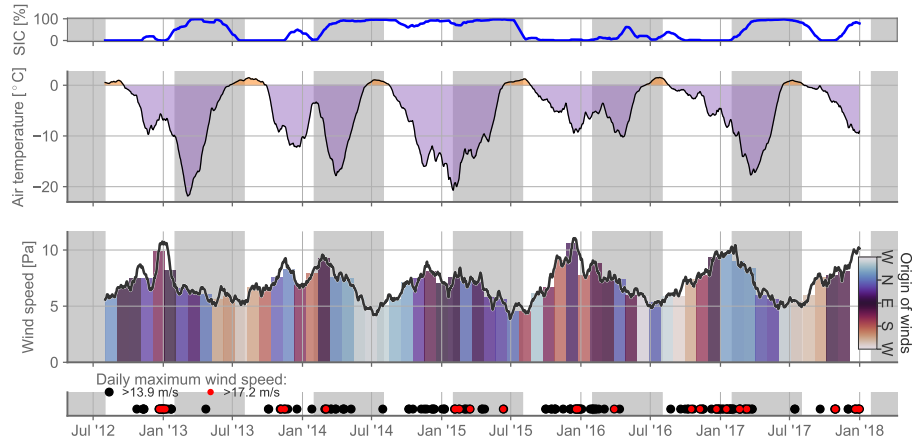


Figure 8: Time series from the mooring site: *a*: Sea ice concentration. *b*: 2-m air temperature from ERA-5. *c*: 10-m wind speed (ERA-5). Wind direction indicated with colored bars. *d*: Storm index showing days where the daily maximum (hourly) ERA-5 10-m wind speed exceeds BF7, 13.9 m/s (black) and BF8, 17.2 m/s (red). A 31-day boxcar filter has been applied in panels *a-c*.

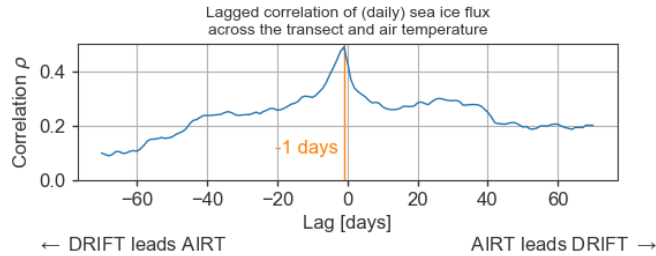


Figure 9: Lagged correlation between daily air temperature and daily sea ice drift across the transect shown in Figure 1c.